ADVANCED FUNCTIONAL MATERIALS
www.afm-journal.de

www.MaterialsViews.com

Surface Investigation on Gd_4M_8 (M = Zn, Ni) Single Molecule Coolers

*Valdis Corradini, Alberto Ghirri, Andrea Candini, Roberto Biagi, Umberto del Pennino, Valentina De Renzi, Gianluca Dotti, Edwige Otero, Thomas N. Hooper, Ross Inglis, Euan K. Brechin, and Marco Affronte**

Proving the preservation of functionality at the molecular scale is still a major challenge, both for the choice of suitable derivatives and protocols and for the employed experimental tools and methods. By using a combined scanning probe (AFM and STM) and spectroscopic methodology (XPS, XAS and XMCD), it is shown that Gd_4M_8 derivatives (with M = Zn^{2+}, Ni^{2+}) are robust molecular units which preserve their electronic, magnetic, and thermodynamic properties when deposited on a metallic surface. Namely, entropy variation $\Delta S = [S(6\ T) - S(0\ T)]$ exceeding 8 R (20 J kg^{-1} K^{-1}) at 4 K in isolated Gd_4Ni_8 molecules dispersed on Au(111) surface is measured and a viable route to exploit large magnetocaloric effect at single molecule level is shown.

1. Introduction

The changes of thermal properties in magnetic materials upon the application of a magnetic field are known as magnetocaloric effects (MCE). Of particular interest for applications are substances for which the magnetic entropy decreases when a magnetic field is applied. In these cases, an adiabatic demagnetization process provokes a temperature drop, that is a cooling process driven by the magnetic field. Though MCE are present in all magnetic materials, the interest for applications is obviously focused on substances with large entropy variation upon application of relatively small magnetic fields. Paramagnetic impurities in alloys or salts are used as coolers at cryogenic temperatures while crystalline materials with concomitant magnetic and structural transitions are intensively studied as magnetic refrigerants up to room temperature. Both these classes of materials cannot be simply efficiently scaled at the nanometer size since in the first case (paramagnets) the density of magnetic materials is too small, whilst in the second one the long range order is less effective –or disappears- in small objects. Nanomagnets and in particular magnetic molecules emerged in the last decade as an alternative route for refrigeration at cryogenic temperatures since they may offer high magnetization and large values of entropy change.[1] To make this possible, we considered molecules with high spin ground states and small anisotropies that show record values of entropy variation density as compared to other substances, including intermetallic alloys, at cryogenic temperatures. So far studies have been carried out on bulk samples but a key question—whether giant values of entropy variation can be obtained at the nano- or even molecular scale—has not been faced yet. To answer this question requires overcoming several key challenges: in first instance, we have to find suitable magnetic molecules that can be safely dispersed as individual objects in a matrix or on surfaces while preserving their high MCE; secondly we have to find a suitable experimental tools to probe the magnetic properties at the single molecule level. Here, we have focused our attention on Gd-based molecular clusters which are of potential interest for refrigeration at cryogenic temperatures. Among these, the recently synthesized family of Gd_4M_8 (M = transition metal) derivatives have shown, on bulk measurements, large MCE due to the high spin value and low anisotropy of the trivalent Gd ions, while the possibility to change the divalent d-metal allows us to tune their cooling performances in the range of temperature of interest (1–4 K).[2]

We report a spectroscopic investigation on individual Gd_4M_8 molecules dispersed on a substrate. We use X-ray absorption and circular dichroism that are very sensitive and element selective techniques to probe the magnetic properties of molecules dispersed on gold and highly ordered pyrolytic graphite (HOPG). Au(111) surface is chosen as a test bed since interaction with a metallic surface can be detrimental, while tests on the less reactive HOPG are also carried out for comparison and reported in the Supplementary Information. Using combined experimental techniques (STM, AFM, XPS, XAS, and

Dr. V. Corradini, Dr. A. Ghirri, Dr. A. Candini
S3 Centre, Institute Nanoscience – CNR
via G. Campi 213/A 41125, Modena, Italy
Dr. R. Biagi, Prof. U. del Pennino, Dr. V. De Renzi, Dr. G. Dotti, Prof. M. Affronte
Dipartimento di Scienze Fisiche Informatiche e Matematiche
Università di Modena e Reggio Emilia and S3 Centre
Institute Nanoscience-CNR
via G. Campi 213/A 41125, Modena, Italy
E-mail: marco.affronte@unimore.it
Dr. E. Otero
Synchrotron SOLEIL
L'Orme des Merisiers
91120, Saint-Aubin, France
Dr. T. N. Hooper, Dr. R. Inglis, Prof. E. K. Brechin
EaStCHEM School of Chemistry
The University of Edinburgh
West Mains Road, Edinburgh EH93JJ, UK

DOI: 10.1002/adfm.201400460

XMCD), we show that the molecules remain intact and that they preserve their magnetic properties, including MCE, when dispersed on these substrates. This conclusion is obtained by direct comparison of results obtained on sub-monolayers (ML) and thick films (TF) of the same derivative. We first consider the case of Gd_4Zn_8 to isolate the magnetism of the Gd_4 core (Zn being diamagnetic) and then consider the case of Gd_4Ni_8 which exhibits a large MCE in bulk measurements. These results are unique, since previous experiments have shown that molecules can lose their symmetry (with a reduction of the MCE) when deposited on surfaces.[3] Moreover extraction of information from XMCD spectra is non-trivial, requiring some precautions when comparing results with data obtained from bulk magnetization measurements. Herein we report an appropriate protocol.

2. Experimental Results

2.1. Deposition and Morphological Characterization

The synthesis and characterization of molecular derivatives $[Gd_4Ni_8(OH)_8(hmp)_8(O_2CEt)_8(MeOH)_6][ClO_4]_4$ (Gd_4Ni_8 in short, see **Figure 1**a,b for molecular features) and $[Gd_4Zn_8(OH)_8(hmp)_8(O_2C^iPr)_8][ClO_4]_4$ (Gd_4Zn_8 in short) studied in this paper are reported in reference [2]. Here hmp-H = 2-(hydroxymethyl)pyridine) = C_6H_7NO. The core of the molecule consists of a square of four corner-sharing $\{Gd^{III}_2M^{II}_2O_4\}$ cubanes. The shared corners are the Gd ions which thus themselves form an inner $\{Gd^{III}_4\}$ square, each edge of which is occupied by two μ3-OH- ions which further bridge to a M^{2+} ion. The μ3-L- ions chelate the M^{2+} ions and use their O-arm to further bridge to the second M^{2+} ion in the same cubane and to one Gd ion. There are two carboxylates per cubane, each μ-bridging across a M^{2+}...Gd square face, alternately above and below the plane of the $\{Gd^{III}_4\}$ square. Both derivatives are soluble in dichloromethane (DCM) and since there is no particular interest in controlling orientation/magnetic anisotropy, we used a liquid phase method to deposit them on substrates. No functional linker was used to anchor the molecules on surfaces since these may weaken the thermal coupling. By a combined XPS, AFM, and STM investigation we firstly derived the best conditions to obtain a two-dimensional distribution of Gd_4M_8 on surfaces: the Au(111) surface was immersed for 10 min in a 10^{-5} M solution of Gd_4M_8 in DCM, then rinsed for 10 s in DCM and blow dried in a flux of nitrogen gas. In this way a uniform sub-ML of isolated Gd_4M_8 molecules is obtained as evidenced by STM. From the statistical analysis of the STM images (see Figure S1 in the Supporting Information, S.I.), we derived that approximately 20–30% of the surface was covered by Gd_4M_8 clusters. STM images show no aggregation of the molecules which, for the concentrations used, are well separated and in direct contact with the gold surface (Figure 1c). STM images were taken at room temperature and low tunneling current (30 pA): the high cluster mobility during the tip sweep indicates that the molecules are weakly bonded on the Au surface, probably by simple van der Waals (vdW) interactions. From the STM line-profiles (Figure 1d), we reproducibly found an average lateral size of 3.0 ± 1.0 nm and a height of 1.0 ± 0.5 nm, close to the dimensions of the single Gd_4M_8 molecule (diameter of 2.0 nm and height of 1.0 nm) as determined by structural crystallographic analysis (see Figure 1a,b), convoluted with the dimension of the tip. From STM images we cannot derive any particular orientation although it is reasonable to expect that molecules tend to lie flat on the surface as induced by the vdW interaction.

AFM images (see Figure S2 in S.I.) were taken on molecules dispersed on HOPG using the same protocol except that no rinsing and blow drying in a flux of nitrogen gas was used, since the molecule-graphite bond is even weaker than with gold. A uniform distribution of Gd_4M_8 molecules was obtained as evidenced by AFM images (see Figure S2 in S.I.). From a statistical analysis of the AFM images, we derived that approximately 5–15% of the surface was covered by Gd_4M_8 clusters, consistent with previous results on gold. AFM images (see Figure S2 in S.I.) show the formation of small aggregates with reproducible height of 3.0 ± 0.5 nm that indicates stacking of two-three molecules.

2.2. XPS Investigation

In **Figure 2** the Gd-3d, Ni-2p, N-1s and O-1s core level spectra of the Gd_4Ni_8 ML deposited from liquid-phase on the Au(111) and HOPG surfaces are plotted along with their line shapes nicely reproduce the corresponding ones obtained on thick film (TF). For all core levels the line shapes of the ML's and TF are

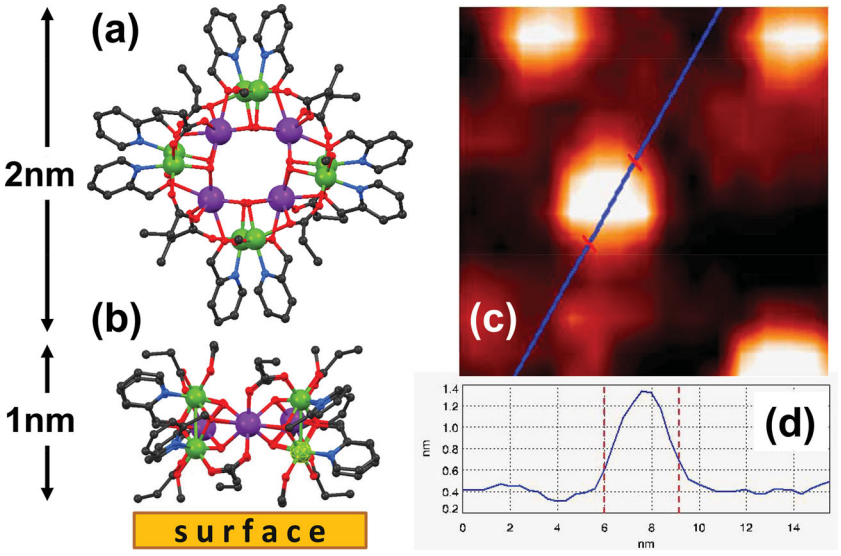

Figure 1. a,b) Molecular structure, dimensions and orientation of the Gd_4M_8 cluster with respect to the surface. Colour scheme: Gd, large purple circles; M(= Zn, Ni), green; O, red; N, blue; C, black. c) STM image (12 nm × 11 nm) (2.0 V, 30 pA) of a sub-ML of Gd_4Ni_8 deposited on Au(111) surface, and d) line-profiles taken along the directions indicated.

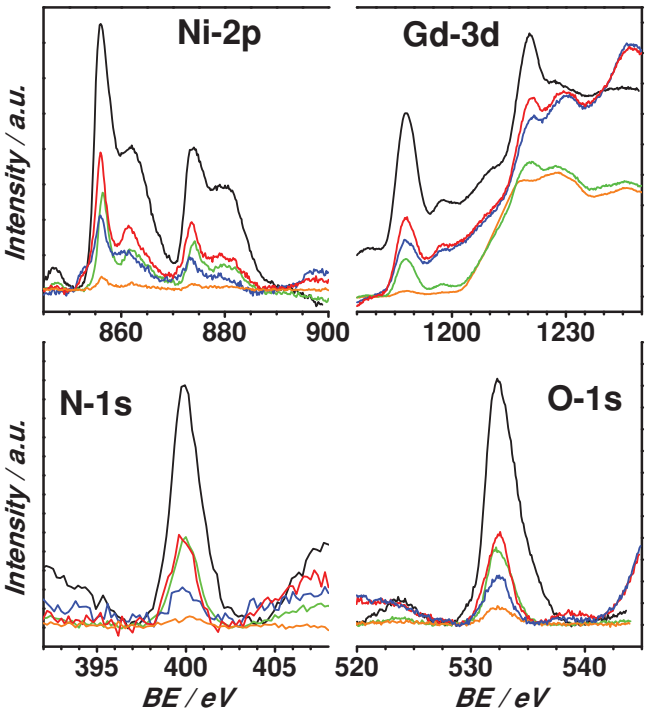

Figure 2. XPS core level spectra obtained after immersing the Au(111) substrate for 10 min in DCM solutions with different molecular concentrations: 10^{-4} M (red line), 10^{-5} M (blue line). HOPG in 10^{-4} M (green line), 10^{-5} M (orange line) concentrations of Gd_4Ni_8. The corresponding spectra taken on thick films (black line) are shown for comparison.

quite similar. The stoichiometric ratios Gd/(8Ni), N/(8Ni) and O/(8Ni) are reproducible (see Table S1 in S.I.) and close to the expected ones (4, 8 and 54 respectively), proving the chemical stability of the molecular core. In particular the Gd ions are eight coordinate and in square antiprismatic geometries whilst the Ni ions are six-coordinated but the geometry is rather distorted octahedral. From the Au-4f/Gd-3d ratio (and taking into account the attenuation of gold signal due to the overlayer) we derive the Gd_4Ni_8 coverage reported in Table S1 (S.I.), in agreement with the values obtained from STM.

2.3. XAS and XMCD Investigation

To further check the integrity of the metal core of the molecule, we compared the Gd-$M_{4,5}$ and Zn-$L_{2,3}$ (Ni-$L_{2,3}$) X-ray adsorption spectra (XAS) collected on the Gd_4Zn_8 (Gd_4Ni_8) ML on Au(111) with the corresponding spectra obtained on the TF (**Figure 3**a,b). We avoided sample degradation, that could be induced by radiation exposure, by working at very low flux (below 10^{10} photons s^{-1}) and by strictly monitoring XAS spectra throughout the experiments. The XAS spectra of the MLs perfectly match those obtained on TF. This confirms that the interaction with the gold surface does not affect the valence electronic structure of the Gd_4M_8 (M = Zn, Ni) molecular core: namely, the oxidation state for Gd and Zn (Ni) and the ligand-field at the Zn (Ni) site is preserved. This implies that the zinc (nickel) ions are divalent while gadolinium ions are trivalent.

The dichroic XMCD signal (expressed in%) is evaluated by taking the difference between the two XAS spectra obtained with different x-ray polarizations ($\sigma^{\uparrow\downarrow} - \sigma^{\uparrow\uparrow}$) and dividing by the height of the average of the two polarizations. Not only are the shapes of the XMCD spectra essentially the same for TF and ML but the relative intensities of XMCD signals also coincide. Note that the XMCD values expressed in percentage (%) do not depend on the amount of the derivative analyzed, thus the signal on ML can be directly compared with that obtained on TF, whilst the quantification of the dichroic signal in terms of

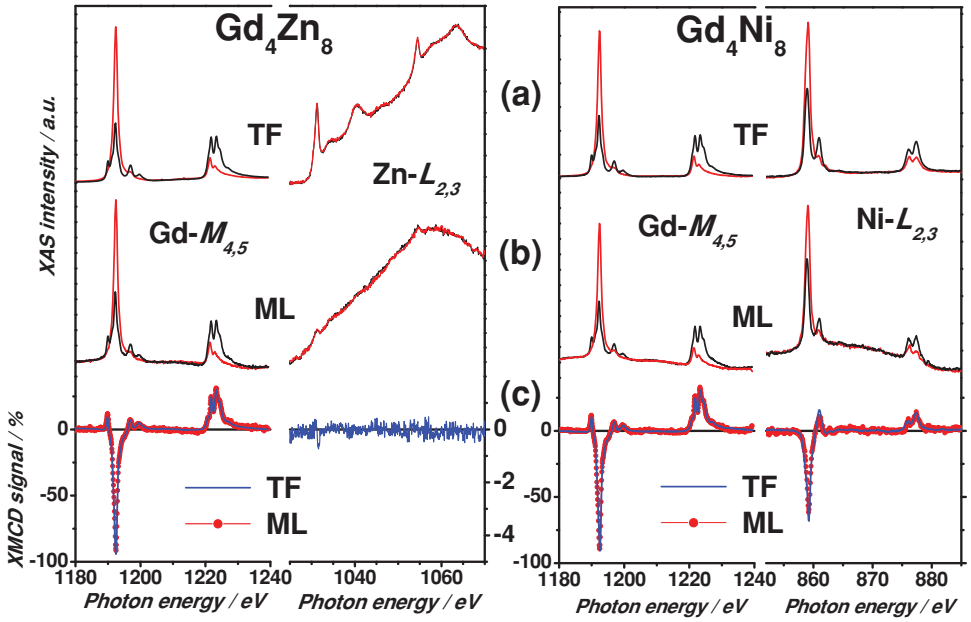

Figure 3. Gd-$M_{4,5}$ and Zn-$L_{2,3}$ (left panel) (Ni-$L_{2,3}$ right panel) absorption spectra taken using both photon helicities with the relative dichroic signal (c) measured at 3 K and 6 T for the ML of Gd_4Zn_8 (Gd_4Ni_8) on Au(111) (b) and the corresponding TFs (a). The Zn XMCD for the ML (not shown) is zero within an error-bar for the noise of ±5%.

absolute magnetic moments is not straightforward. According to that reported in the literature for Gd^{3+} ions in O_h symmetry,[4] we started by assuming that the area of the XMCD curve is proportional to the magnetization. We also checked that the shape of the dichroic signal does not change with temperature and magnetic field (see Figure S4 in S.I.), therefore the height of the M_5 peak at 1192 eV can be considered proportional to the area of the dichroic signal. We can therefore obtain fast detection of the dichroic signal by simply measuring the edge (E) and pre-edge (P) intensities $[(E\sigma^{\uparrow\downarrow} - P\sigma^{\uparrow\downarrow}) - (E\sigma^{\uparrow\uparrow} - P\sigma^{\uparrow\uparrow})]/1/2[(E\sigma^{\uparrow\downarrow} - P\sigma^{\uparrow\downarrow}) + (E\sigma^{\uparrow\uparrow} - P\sigma^{\uparrow\uparrow})]$ when the magnetic field is swept in isothermal conditions. Here E is the intensity of the XAS at the energy which correspond to the maximum of the XMCD signal and P is the level of the background preceding the absorption edge.

Since the dichroic signal at the Zn site is vanishingly small, the total magnetization of the whole Gd_4Zn_8 molecule is very close to the Gd magnetic moments. In **Figure 4**a we report the dichroic signal (%) as a function of the applied magnetic field (up to 6 T) at different temperatures (from 3 K to 15 K) measured on a ML of Gd_4Zn_8 on the Au surface, together with the corresponding signal taken on the TF. We expect the actual temperature of the molecules to be slightly higher (10%) than that measured by our thermometer in direct contact with the substrate, and this discrepancy can be occasionally larger for the lowest working temperature. Within this estimation, the behaviour of isolated molecules (ML) is reproducible and the systematic change with temperature matches that measured on the corresponding TF (Figure 4a).

In **Figure 5**a,b we report the dichroic signals (%) at the Gd-$M_{4,5}$ and Ni-$L_{2,3}$ edges as a function of the applied magnetic field (up to 6 T) at different temperatures (from 3 K to 15 K) measured on the ML of Gd_4Ni_8 on the Au surface and the corresponding spectrum taken on TF. Again, the plot shows that the behaviour of isolated molecules (ML) perfectly matches that observed for the TF, allowing us to conclude that not only the electronic features but also the magnetic properties of both Gd_4M_8 derivatives are preserved.

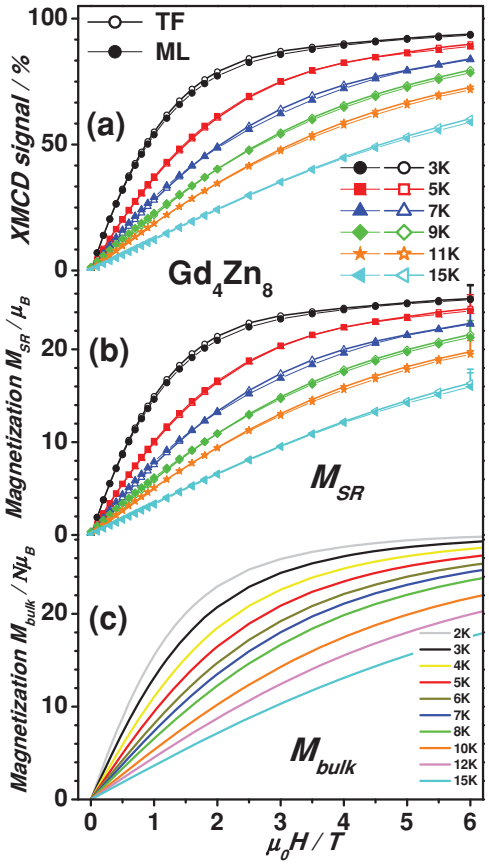

Figure 4. (a) XMCD signal (%) measured as a function of magnetic field at different temperatures (from 3 K to 15 K) for the Gd_4Zn_8**TF** and for the **ML** on Au(111). (b) Magnetization M_{SR} curves obtained by XMCD data by applying the sum rules at the Gd-$M_{4,5}$ edge for each temperature at the maximum field (6T). Error bar account for the uncertainty in the T_Z and SC parameters used in the sum rules (see the discussion in the manuscript). The fact that M_{SR} is 8% smaller than M_{bulk} is within experimental error due to our choice of both T_Z and SC parameters. (c) Magnetization $M(H)$ curve measured on bulk microcrystalline Gd_4Zn_8 powder by conventional DC magnetometry.

2.4. Estimation of Magnetization by Sum Rules

In order to get more quantitative information and compare XMCD data with magnetization measurements on bulk samples, we now apply the XMCD sum rules.[5,6] The magnetization of the Gd_4Zn_8 molecule is given by the magnetic moment of four Gd ions while for the Gd_4Ni_8 we have to sum the magnetic contributions of four Gd and eight Ni ions. Since XMCD spectra are identical for ML and TF (see Figure 3c), analysis of the XMCD spectra is the same for both cases. Note also that the XAS and XMCD spectra of Gd measured on Gd_4Zn_8 and Gd_4Ni_8 molecules also overlap each other (see Figure 3) and thus data analysis is the same for the two derivatives.

According to the sum rules,[7] the average values of the spin (m_S) and orbital (m_o) magnetic moments (along the magnetic field z-direction) for Gd are given by:

$$\frac{m_o}{\mu_B} = -\frac{2qN_{eff}}{r} \quad \frac{m_S}{\mu_B} = -\frac{(5p-3q)N_{eff}}{r}SC + \frac{6\langle T_Z\rangle}{\mu_B} \qquad (1)$$

Where μ_B is the Bohr-magneton, N_{eff}, is the number of holes in the 4f shell (7 for Gd^{3+}), T_Z is the intra-atomic magnetic dipole term, SC is the spin correction factor, r is the integral of the whole absorption spectrum, $p = A$ and $q = A + B$ where A and B are the integrals of the dichroic signal at the M_5 and M_4 Gd-edges, respectively (**Figure 6**, left panel). The q value of the dichroic signal at the Gd-$M_{4,5}$ edges is related to the orbital moment m_o of the Gd^{3+} ions. As reported in literature, we find that q vanishes and this indicates a complete quenching of m_o due to the crystal field. It turns out that Gd^{3+} ions have only spin moment m_S and a nearly spin-only gyromagnetic factor ($g = 2.0$). It is worth stressing that deposition on the Au surface does not affect the degree of quenching of the orbital momentum. For a Gd^{3+} ion T_Z is expected to be small, approximately 1% of m_S ($6T_Z / m_S = -0.01$).[4] For distorted symmetries larger corrections should be considered but since we have a collection of disordered (or only partially oriented) molecules, we take $T_Z = 0$. For the *SC* factor, which accounts

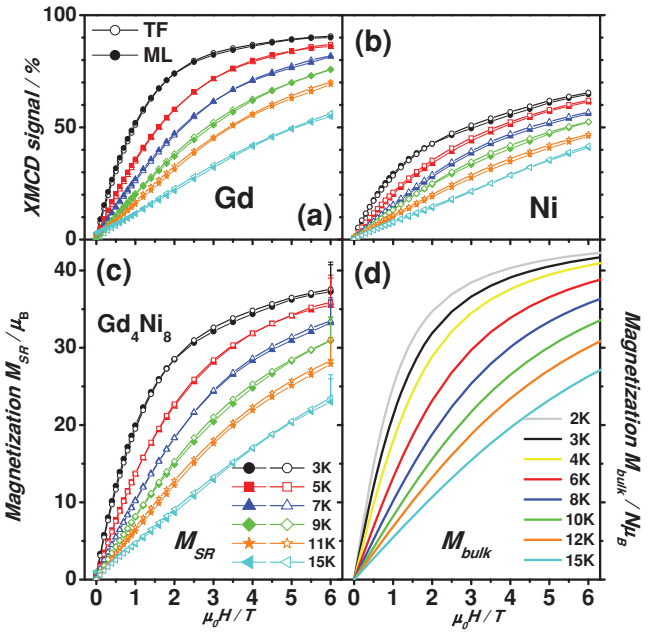

Figure 5. XMCD signals (%) for (a) Gd and (b) Ni measured as a function of field at different T (from 3 K to 15 K) for Gd_4Ni_8 **TF** and **ML** on Au(111). (c) Magnetization M_{SR} curves (in μ_B) of the Gd_4Ni_8 molecule obtained by applying the sum rules at the Gd-$M_{4,5}$ and Ni-$L_{2,3}$ edges for each temperature at the maximum field (6 T) and summing up the contribution from 4Gd + 8Ni ions. The error bars account for the uncertainty in the T_Z and SC parameters used in the sum rules (see the discussion in the manuscript). The fact that M_{SR} is smaller by 10% than M_{bulk} is within experimental error due to our choice of both T_Z and SC parameters. (d) Magnetization M_{bulk} curve measured on bulk microcrystalline Gd_4Ni_8 powder by DC magnetometry.

for the overlapping of M_4 and M_5 edges, theoretical calculations predict SC values up to 1.05 for Gd^{3+}.[4] To convert XMCD data into magnetization values, we considered $SC = 1$ while the uncertainty in both T_Z and SC is visualized by the vertical error bars in the magnetization curves M_{SR} plotted in Figure 4b,5c. For direct comparison with bulk, we report the M_{bulk} curves measured on Gd_4Zn_8 powders by DC magnetometry in Figure 4c: the magnetization M_{SR} estimated by applying the sum rules to XMCD signal reproduces the bulk magnetization M_{bulk}. Overall, considering both the absolute values of M_{SR} and its T- and H-dependence, we conclude that the magnetization measured on isolated Gd_4Zn_8 molecules reproduces that measured on bulk samples very well.

Similarly, we apply the XMCD sum rules at the Ni-$L_{2,3}$ edges to evaluate the Ni magnetic moment (Figure 6, right panel):[7]

$$\frac{m_o}{\mu_B} = -\frac{4qN_{eff}}{3r} \quad \frac{m_S}{\mu_B} = -\frac{(6p-4q)N_{eff}}{r}SC + \frac{7\langle T_Z\rangle}{\mu_B} \tag{2}$$

where N_{eff}, is the number of holes in the 3d shell (is 2 for Ni^{2+}), r is the integral of the whole absorption spectrum, $p = A$ and $q = A + B$ where A and B are the integrals of the dichroic signal at the L_3 and L_2 edges of Ni, respectively. In this case q value does not vanish and this indicates that the partial quenching of orbital Ni moment in both the TF and the ML is an intrinsic property of the ligand field of the molecule. This implies that the Ni^{2+} ions have an orbital moment $m_o \approx 10$–15% of the spin m_S and a gyromagnetic factor, $g = 2.2$. For a Ni^{2+} in O_h symmetry the T_Z term is also expected to be small, approximately 1% of m_S with a maximum of 3% in the case of distorted symmetry ($7T_Z / m_S = -0.01/-0.03$).[8–10] The coordination around each Gd^{3+}, Ni^{2+} site is not perfectly octahedral as shown by the structure of the molecule (Figure 1a,b). Yet, since we have to average over a collection of disordered molecules we also take $T_Z = 0$ for Ni^{2+}. Theoretical calculations, performed as a function of the crystal field (10 Dq), affords SC correction factors for Ni^{2+} ranging between 1 and 1.1.[8–10] We choose SC = 1 to evaluate M_{SR}, while the uncertainty in both the T_Z and SC value is visualized by the error bars in Figure 5c. The M_{SR} of the whole Gd_4Ni_8 molecule, obtained by summing all the gadolinium and nickel (4Gd+8Ni) contributions, is plotted in Figure 5c and can be compared with the magnetization curves measured on bulk microcrystalline powders M_{bulk} (Figure 5d). This, along with the matching of the overall temperature and magnetic field dependencies, lead us to conclude that M_{SR} also reproduces the M_{bulk} Gd_4Ni_8 rather well.

2.5. Evaluation of MCE

Based on the magnetization curves reported in Figure 4b, 5c and taking the correspondence between the dichroic signal and the absolute value of the magnetization as discussed above, we now use the entropy change ΔS_m between different magnetic fields at different temperatures by using the conventional Maxwell equations to estimate the entropy change ΔS_m between different magnetic fields at different temperatures:

$$\Delta S_m(T)_{\Delta H} = \int_{H_i}^{H_f}\left[\frac{\partial M(T,H)}{\partial T}\right]_H dH \tag{3}$$

Where H is the applied magnetic field and M(T,H) the magnetization measured at different temperature T and fields: the derivative $\partial M/\partial T$ is numerically evaluated by experimental values at fixed magnetic field H.

Results for both TF and ML are plotted in **Figure 7** for $\mu_0\Delta H =$ 6 T – 0 T and they can be compared with similar results obtained for crystalline samples. ΔS_m for TF and ML reproduce that measured in the bulk samples within the uncertainty due to the sum rules parameters, visualized by the error bars. In both TF and ML, a clear identification of the maximum of ΔS_m vs T - visible in the bulk - is impossible also due to the limited number of experimental data available at low temperature. Remarkably, for Gd_4Ni_8, $\Delta S = S(6\text{ T}) - S(0\text{ T})$ exceeds 8R (20 J kg^{-1} K^{-1}) at 4 K, where $R = 8.314$ J mol^{-1} K^{-1} is the gas constant.

3. Final Remarks

In this work we reported a viable route to establishing large magnetocaloric effects at the single molecule level. Some steps of our protocol merit further discussion.

The integrity of the molecule (structure and electronic properties) was initially tested by scanning probe (AFM and STM)

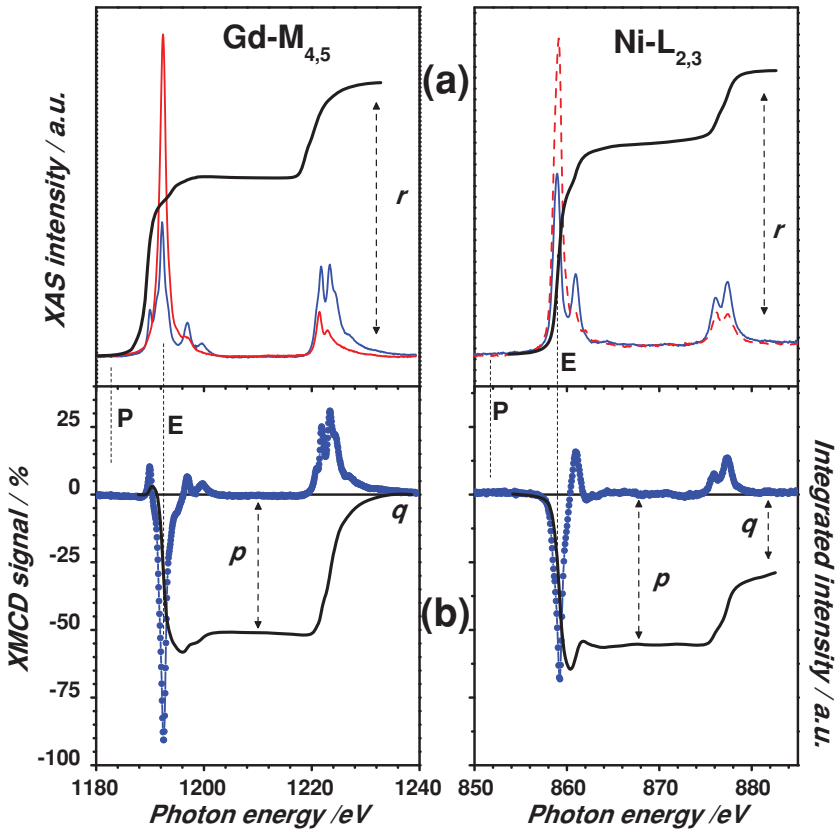

Figure 6. (a) Gd-$M_{4,5}$ and Ni-$L_{2,3}$ XAS spectra taken with $\sigma^{\uparrow\downarrow}$ and $\sigma^{\uparrow\uparrow}$ circularly polarized light at 3 K, 6 T, and the XAS integral (thick lines) for the Gd_4Ni_8**TF**. (b) XMCD ($\sigma^{\uparrow\downarrow} - \sigma^{\uparrow\uparrow}$) spectra (dotted lines) and their integrals (thick lines). E and P represent the edge and pre-edge positions. *p* and *q* are the values of the integrals used for the sum rules analysis.

and XPS as well as by X-ray absorption. Comparison of the dichroic spectra obtained on sub-ML and TF allowed us to conclude that the magnetic behavior as a function of temperature and magnetic field is preserved when Gd_4M_8 (M = Zn, Ni) molecules are deposited on Au(111) and HOPG surfaces. This is the key result of our work. Further data analysis is needed to directly compare MCE values obtained on molecules dispersed on surfaces with measurements on bulk samples. The use of the sum rules is well consolidated in literature, although the parameters in Equation (1),(2) ultimately depend on the actual features of the ligand field of Gd and Ni. T_Z and SC parameters reported in the literature may change by up to 10% and we take this as reasonable uncertainty in the determination of M_{SR}. The sum rules allow us to evaluate the absolute magnetization values M_{SR} at different temperatures and applied magnetic fields. These, in turn, have been used to evaluate the entropy change and therefore the MCE.

The use of magnetization data is an indirect method commonly used the literature to evaluate MCE for bulk samples. Deeper analysis would require low-temperature specific heat measurements or, even better, experiments involving an adiabatic demagnetization process to evaluate the effective temperature change under real experimental conditions. Note that the ΔS value we have evaluated here perfectly matches that estimated from both specific heat and magnetization measurements on bulk samples reported elsewhere.[2] The effective cooling power and temperature variation would depend on the specific working conditions, namely the total heat capacity of the system to be cooled and the thermal conductivity of the linker between the molecule and its environment. These and other factors need to be taken into account in order to exploit the MCE of dispersed molecular units and direct measurements (adiabatic demagnetization) are certainly required for a correct evaluation of the effective cooling power of a specific device, but this is clearly beyond the scope of our present work.

Gd-based molecules have been shown to be excellent coolants at cryogenic temperatures.[1] Among these, the family of Gd_4M_8 (M = Zn, Ni, Co, Cu) represent a flexible template for which optimal conditions for MCE can be found by changing both the divalent *d*-metal and the bridging ligand.[2] Here, we showed that Gd_4M_8 (M = Zn, Ni) are also robust enough to be dispersed on surfaces. Preliminary spectroscopic results on the Gd_4Co_8 derivative of the same family show that (the redox-active) Co is more sensitive to the metallic Au surface thus telling us once more that the effects of deposition on a surface must be evaluated on a case by case basis.

Finally it is worth to remembering that crystals of molecular nanomagnets have already shown record MCE values as compared to other bulk materials at cryogenic temperatures if the MCE is expressed in the same units (J kg^{-1} K^{-1}).[1] It is not clear how other non-molecular materials can work as coolants at the nanoscale, but here we demonstrate that molecular clusters may work rather efficiently as independent cooler units.

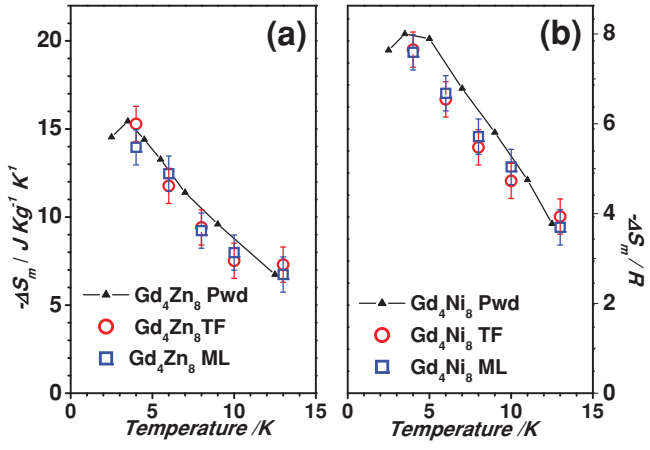

Figure 7. (a) Entropy change ΔS_m vs T estimated for $\mu_0\Delta H$ = 6 T – 0 T as derived from the isothermal M_{SR} curves of Figure 4 for the Gd_4Zn_8**TF** and **ML** compared with bulk microcrystalline powders. (b) Entropy change ΔS_m vs *T* calculated for $\mu_0\Delta H$ = 6T-0T, derived from the isothermal M_{SR} curves of Figure 5 for the Gd_4Ni_8**TF** and **ML** compared with bulk microcrystalline powders.

4. Experimental Section

Sub-monolayers (ML) were obtained by immersing the HOPG, Au(111) single crystal or the Au/mica flamed-annealed surface in a mM solution of Gd_4M_8 using dichloromethane (DCM) as solvent and blow dried in flux of nitrogen gas. Thick films (TF) were obtained by drop casting the saturated solution on the same substrates.

STM, AFM, and XPS were used to check that the desired two dimensional distribution of nanometric entities was actually obtained. Electrochemically etched tungsten wires were used as tips. Room temperature STM image acquisition was carried out in constant current mode with typical conditions of 2.0 V and the lowest achievable current (30 pA) in order to minimize dragging and damaging of the soft organic materials by the scanning tip.

XPS measurements were performed using an Omicron hemispherical analyzer (EA125) and a non-monochromatized Mg-Kα X-ray source ($h\nu = 1253.6$ eV).

Soft XAS and XMCD measurements were performed at the DEIMOS beamline of SOLEIL Synchrotron Radiation Facility (France). The lowest sample temperature reached was ≈3 K and the base pressure of the experimental chamber 1.0×10^{-10} mbar. We paid close attention to avoid any sample degradation induced by radiation exposure, working at very low flux (below 10^{10} photons/s) and by strictly monitoring XAS spectra throughout all the experiments for detecting even the smallest traces of sample damaging. XMCD measurements at the Gd-$\mathbf{M}_{4,5}$, Zn-$\mathbf{L}_{2,3}$, Ni-$\mathbf{L}_{2,3}$ edges were performed in total electron yield mode using circularly polarized light with ≈100% polarization rate and with external magnetic fields $\mu_0\mathbf{H}$ up to 6T, applied perpendicular to the sample surface and parallel to the incident photon beam. The dichroic spectrum is the difference between the XAS spectra taken with the helicity of the incident photon antiparallel ($\sigma^{\uparrow\downarrow}$) and parallel ($\sigma^{\uparrow\uparrow}$) to the applied magnetic field ($\mathbf{H}$). In order to minimize the effects of field inhomogeneity, we carried out measurements by switching both the helicities and the applied field. The $\sigma^{\uparrow\uparrow}$ ($\sigma^{\uparrow\downarrow}$) absorption spectra are therefore the average spectra collected with the helicity parallel (antiparallel) to $\mathbf{H}$.

Magnetization measurements on bulk polycrystalline samples were carried out using a commercial PPMS (Quantum Design) using the extraction method.

Acknowledgements

The XAS and XMCD measurements were performed on the DEIMOS beamline, using the Chemistry 1 support laboratory, at SOLEIL Synchrotron (proposal number 20110850). The MBE chamber used during our beamtime on DEIMOS has been funded by the Agence National de la Recherche; grant ANR-05-NANO-073. The authors are grateful to Fadi Choueikani, Philippe Ohresser and to DEIMOS staff for assistance and to the SOLEIL staff for smoothly running the facility. EKB thanks the EPSRC for financial support.

Received: February 10, 2014
Revised: March 24, 2014
Published online: May 5, 2014

[1] M. Evangelisti, in *Molecular Magnets, Physics and Applications* (Eds: J. Bartolomé, et al.) Springer-Verlag, Berlin Heidelberg **2014**, p 365.
[2] T. N. Hooper, J. Schnack, S. Piligkos, M. Evangelisti, E. K. Brechin, *Angew. Chem. Int. Ed.* **2012**, *51*, 4633.
[3] V. Corradini, A. Ghirri, A. Candini, R. Biagi, U. del Pennino, G. Dotti, E. Otero, F. Choueikani, R. J. Blagg, E. J. L. McInnes, M. Affronte, *Adv. Mater.* **2013**, *25*, 2816.
[4] Y. Teramura, A. Tanaka, B. Thole, T. Jo, *J. Phys. Soc. Jpn.* **1996**, *65*, 3056.
[5] B. T. Thole, P. Carra, F. Sette, G. van der Laan, *Phys. Rev. Lett.* **1992**, *68*, 1943.
[6] J. Stohr, *J. Magn. Magn. Mater.* **1999**, *200*, 470.
[7] C. T. Chen, Y. U. Idzerda, H. J. Lin, N. V. Smith, G. Meigs, E. Chaban, G. H. Ho, E. Pellegrin, F. Sette. *Phys. Rev. Lett.* **1995**, *75*, 152.
[8] Y. Teramura, A. Tanaka, T. Jo, *J. Phys. Soc. Jpn.* **1996**, *65*, 1053.
[9] C. Piamonteze, P. Miedema, F. M. de Groot, *Phys. Rev. B* **2009**, *80*, 184410.
[10] J. P. Crocombette, B. T. Thole, F. Jollet, *J. Phys.: Condens. Matter* **1996**, *8*, 4095.